COMPUTER VISION AND IMAGE UNDERSTANDING
Vol. 66, No. 2, May, pp. 223–232, 1997
ARTICLE NO. IV970608

Deformations Incorporating Rigid Structures

J. A. Little, D. L. G. Hill, and D. J. Hawkes

Division of Radiological Sciences, 3rd Floor Guy's Tower, Guy's Hospital, London Bridge, London SE1 9RT, United Kingdom

Received August 20, 1996; accepted December 15, 1996

Medical image registration algorithms invariably assume that the objects in the images can be treated as a single rigid body. In practice, some parts of a patient, usually bony structures, may move as rigid bodies, while others may deform. To address this, we have developed a new technique that allows identified objects in the image to move as rigid bodies, while the remainder smoothly deforms. The transformation is based on a radial basis function solution with a basis function modified by use of distance transforms based on rigid structures within the image. These distance transforms are also used to form an underlying transformation which ensures an interpolating solution. The resulting deformation technique is valid in any dimension, subject to the choice of the basis function. We demonstrate this algorithm in two dimensions on illustrative images as well as on sagittal magnetic resonance images collected from a volunteer.

1. INTRODUCTION

In recent years it has become increasingly common to register images of a patient acquired either at different times on the same imaging modality or by using multiple imaging modalities for the purposes of clinical evaluation. There have been numerous reviews of this topic, including [1–4]. The majority of methods focus on the head as it is usually valid to assume that the brain will behave as if it were a single rigid body [5–8]. This is, however, rarely the case when matching images of anatomy outside of the head. For multiple images the patient will have moved between acquisitions and soft tissue structures may well have changed shape, hence a deformation will be needed to accurately register the scans together. Here there is quite often patient deformation between scans and a nonlinear approach is more appropriate (see [9]). Even in the head there are cases where the rigid body assumption is not valid. Edwards *et al.* [10] described a clinical case where there was a change in the shape of the brain after a surgical procedure to implant subdural electrodes. In this case neither a rigid body nor a nonlinear thin-plate spline technique recovered the transformation between preoperative and postoperative scans. A composite approach was used in which the image was segmented into two parts and one part of the image deformed while the other was kept rigid. This led to an improvement but added the problem of discontinuity at the segmented object borders.

Using images to guide interventional procedures is a rapidly growing field. At present the interventionalist usually performs the procedure with only a two-dimensional image, typically fluoroscopy, ultrasound, or a single slice of computed tomography (CT), for guidance. Often a preoperative three-dimensional scan, either CT or magnetic resonance (MR), is acquired for planning purposes and displaying this matched to the two-dimensional image would be advantageous. Between the acquisition of the 3D image and the interventional procedure the patient will almost certainly have moved and may even be lying in a different position and so in order to match the images accurately a deformation must take place.

In principle we could build a model of the patient's anatomy which incorporates sufficient detail on mass, elasticity, and viscosity to compute the effect of any distortion to arbitrary accuracy (see, for example, Waters [11]). In practice these calculations are very demanding on computational resources and unlikely to provide a solution of sufficient accuracy in the time scale required for interventional work. We therefore have concentrated our efforts on using interpolation to estimate motion and deformation.

At present the majority of deformation techniques have been developed for patient to patient and patient to atlas image matching and hence assume that all parts of the image being transformed are deformable [12]. For multiple images of a single subject this is rarely the case. These images will be of part of the anatomy which contains both rigid structures, such as bone, as well as soft tissue structures which can deform and change shape. This has led us to develop an algorithm which allows us to constrain parts of an image to move subject to independent rigid body constraints, while allowing the remainder of the image to deform due to both the rigid body transformations and a deformation due to the transformation of user specified landmark points. We define the rigid structures, or objects, by a segmentation of the image. This is at present a user-

1077-3142/97 $25.00

defined segmentation but the method of segmentation has no bearing on the deformation algorithm. We will provide illustrative examples on two-dimensional images in order to show the usefulness of this method.

2. BACKGROUND THEORY

This algorithm is formed by the adaptation and combination of two well-known scattered data interpolation methods into one composite form which will allow us to constrain rigid regions, which can move subject to a user defined rigid body transformation, with a landmark-based deformation. These methods are landmark based interpolation using kriging [13], thin-plate splines [14, 15], or radial basis functions [16, 17], and inverse distance weighted interpolation [18]. Further to these methods we will be using a measure of the distance between points in $\mathbb{R}^d$ and our rigid structures.

2.1. *Point-Based Interpolation*

Point-based interpolation is useful when we are given sparse data from a multidimensional scalar field and we wish to estimate the value of the field at other spatial locations. For example, let us have n sites, $\mathbf{t}_i = (t_i[1], \ldots, t_i[d])^T$, $i = 1, \ldots, n$, in d dimensional space, at each of which we have an observed value x_i. For an interpolating solution we require a function, $f(\mathbf{t})$ say, which maps from $\mathbb{R}^d$ to $\mathbb{R}$ and is exact at the measurement sites, that is that $f(\mathbf{t}_i) = x_i$. Three methods which have been widely used lead to the same functional form for the interpolator despite using different underlying assumptions about the form of the scalar field. These are the kriging, thin-plate spline, and radial basis function approaches. These solutions are arrived at by using different constraints on the behaviour of the interpolator away from the sites [19]. Kriging is a method which provides a best linear unbiased estimate of the solution [13, 20], thin-plate splines minimize a bending energy function [14], and radial basis functions simply provide an exact interpolator at the sites without any minimization constraints [21].

A general interpolating solution using radial basis functions can be formed with two components [20, 22], a linear combination of monomials and a linear combination of basis functions, $\sigma(\mathbf{t}, \mathbf{t}_i)$ say. The monomials represent an underlying drift or mean in kriging and the null space of an energy functional in splines. We can form the basis of this drift in the following manner. First define $\mathbf{p} = (p[1], \ldots, p[d])$ to be a multi-index of nonnegative integers with size given by $|\mathbf{p}| = p[1] + \cdots + p[d]$ and $\mathbf{t}^{\mathbf{p}} = t[1]^{p[1]} \ldots t[d]^{p[d]}$. The rth order monomial drift is spanned by $\mathbf{t}^{\mathbf{p}}$ for $|\mathbf{p}| \le r$. We can represent the drift as $M = ((d + r)!/d!r!)$ functions, $g_1(\mathbf{t}), \ldots, g_M(\mathbf{t})$. For example for $d = 2$ and a linear drift, $r = 1$, we have $M = 3$ and

$$g_1(\mathbf{t}) = 1, \quad g_2(\mathbf{t}) = t[1], \quad g_3(\mathbf{t}) = t[2]. \tag{1}$$

We can write the general form for this type of interpolating solution as ([22], page 31),

$$f(\mathbf{t}) = \sum_{j=1}^{M} a_j g_j(\mathbf{t}) + \sum_{j=1}^{n} b_j \sigma(\mathbf{t}, \mathbf{t}_j). \tag{2}$$

Given the constraints, $f(\mathbf{t}_i) = x_i$, we get n linear equations with the same form as (2) the coefficients of which are given by the solution to the equation

$$\begin{pmatrix} \Sigma & D \\ D^T & 0 \end{pmatrix} \begin{pmatrix} \mathbf{b} \\ \mathbf{a} \end{pmatrix} = \begin{pmatrix} \mathbf{x} \\ 0 \end{pmatrix}, \tag{3}$$

where

$$\begin{aligned} &\mathbf{x}^T = (x_1, \ldots, x_n), \\ &\Sigma_{ij} = \sigma(\mathbf{t}_i, \mathbf{t}_j), \quad i, j = 1, \ldots, n, \\ &D_{ij} = g_j(\mathbf{t}_i), \quad i = 1, \ldots, n, \quad j = 1, \ldots, M \\ &\mathbf{a}^T = (a_1, \ldots, a_M), \quad \mathbf{b}^T = (b_1, \ldots, b_n). \end{aligned} \tag{4}$$

The function $\sigma(\mathbf{t}, \mathbf{t}_i)$ can be either a valid kriging covariance which is dependent on a smoothing parameter α and can be given by (see [13])

$$\sigma_\alpha(\mathbf{t}, \mathbf{t}_i) = \begin{cases} |\mathbf{h}|^{2\alpha}, \alpha \text{ not an integer} \\ |\mathbf{h}|^{2\alpha} \log|\mathbf{h}|, \alpha \text{ an integer} \end{cases} \quad \mathbf{h} \in \mathbb{R}^d,$$

where $\mathbf{h} = \mathbf{t} - \mathbf{t}_i$, or a spline function; see Wahba [22] for a list of valid choices for $\sigma(\mathbf{t}, \mathbf{t}_i)$. An important special case is the thin-plate spline [14], which in two dimensions has $\sigma(\mathbf{t}, \mathbf{t}_i) = |\mathbf{h}|^2 \log|\mathbf{h}|$ and in three dimensions has $\sigma(\mathbf{t}, \mathbf{t}_i) = |\mathbf{h}|$. Further, if no assumptions are made about the behavior of the interpolator away from the constraints then there is a large number of radial basis functions which ensure that there is a solution to (3) [21].

For image deformation we require a multidimensional transfomation defined by a set of points or landmarks. Landmarks are points which have a meaning in the context of the problem under study. Homologous landmarks are pairs of points which can be picked accurately from different images of the same or a similar scene. They are usually one of three types: biological, mathematical, or pseudo-landmarks. Bookstein [23] provides a more detailed discussion of landmark definitions and selection. We now define a deformation based on two sets of homologous landmarks, one on our original image and one on our target or destina-

tion image. Our deformation needs to be exact at these landmarks and a smooth transformation elsewhere.

Instead of sites let us have n landmarks $\mathbf{t}_i = (t_i[1], \ldots, t_i[d])^T$ which we wish to transform to new positions $\mathbf{u}_i = (u_i[1], \ldots, u_i[d])^T$, respectively. We can define a general d dimensional deformation by using d independent interpolators, as defined in (1)–(4), in the following manner:

$$\mathbf{f}(\mathbf{t})^T = (f_1(\mathbf{t}), \ldots, f_d(\mathbf{t})), \tag{5}$$

with constraints

$$f_1(\mathbf{t}_i) = u_i[1], \ldots, f_d(\mathbf{t}_i) = u_i[d], \quad i = 1, \ldots, n. \tag{6}$$

So for any point in $\mathbb{R}^d$ we have a deformation given by

$$\mathbf{t} \to (u[1], \ldots, u[d])^T = \mathbf{f}(\mathbf{t}). \tag{7}$$

Where the individual interpolators are given by

$$f_l(\mathbf{t}) = \sum_{j=1}^{M} a_j[l] g_j(\mathbf{t}) + \sum_{j=1}^{n} b_j[l] \sigma(\mathbf{t}, \mathbf{t}_j), \quad l = 1, \ldots, d \tag{8}$$

with coefficients given by

$$\begin{pmatrix} \Sigma & D \\ D^T & 0 \end{pmatrix} \begin{pmatrix} B \\ A \end{pmatrix} = \begin{pmatrix} U \\ 0 \end{pmatrix}, \tag{9}$$

where

$$\begin{aligned}
&\Sigma_{ij} = \sigma(\mathbf{t}_i, \mathbf{t}_j),\\
&A = (\mathbf{a}_1, \ldots, \mathbf{a}_d), \quad \mathbf{a}_l = (a_1[l], \ldots, a_M[l])^T, \quad l = 1, \ldots, d,\\
&B = (\mathbf{b}_1, \ldots, \mathbf{b}_d), \quad \mathbf{b}_l = (b_1[l], \ldots, b_n[l])^T, \quad l = 1, \ldots, d,\\
&U = (\mathbf{u}_1, \ldots, \mathbf{u}_d), \quad \mathbf{u}_l = (u_1[l], \ldots, u_n[l])^T, \quad l = 1, \ldots, d,\\
&D_{ij} = g_j(\mathbf{t}_i), \quad i = 1, \ldots, n, \quad j = 1, \ldots, M, \quad M = \frac{(d+r)!}{d!r!}.
\end{aligned} \tag{10}$$

In this paper we shall only be using a linear drift so we take $r = 1$ which gives $M = 3$ in two dimensions and $M = 4$ in three dimensions. Further, to ensure that the left-most matrix in (9) is invertible when $r = 1$ we must have at least three noncolinear points in two dimensions or four noncoplanar points in three dimensions.

2.2. *Inverse Distance Weighted Interpolation*

Methods using weights based on a distance measure have been used to solve the interpolation problem. The following is a method proposed by Shepard [18], it is a slightly modified version of this that we shall be using later. This method uses a weighted sum of the constraint values, where the weights are dependent on the distances from the observed point to the constraint sites.

Once again we have a set of n sites, $\mathbf{t}_i = (t_i[1], \ldots, t_i[d])^T$, at each of which we have a value, x_i, of our function. Let our transformation from $\mathbb{R}^d \to \mathbb{R}$ be given by

$$f(\mathbf{t}) = \sum_{i=1}^{n} w_i(\mathbf{t}) x_i, \tag{11}$$

where $f(\mathbf{t}_i) = x_i$, $i = 1, \ldots, n$ are our data constraints. In order that our constraints are satisfied we require a set of weights which have the following properties:

$$\begin{aligned}
&w_i(\mathbf{t}_i) = 1, \quad i = 1, \ldots, n,\\
&\sum_{i=1}^{n} w_i(\mathbf{t}) = 1, \quad \mathbf{t} \in \mathbb{R}^d,\\
&w_i(\mathbf{t}) \geq 0, \quad i = 1, \ldots, n, \quad \mathbf{t} \in \mathbb{R}^d.
\end{aligned} \tag{12}$$

Shepard [18] put forward the weight function

$$w_i(\mathbf{t}) = \frac{q_i(\mathbf{t})}{\sum_{j=1}^{n} q_j(\mathbf{t})}, \tag{13}$$

where

$$q_i(\mathbf{t}) = \frac{1}{s_i(\mathbf{t})^{\mu}}, \tag{14}$$

with $s_i(\mathbf{t})$ being the distance from $\mathbf{t}$ to site $\mathbf{t}_i$. The smoothness of this interpolation scheme is governed by the choice of μ. A value of $\mu > 1$ ensures that the first derivative is continuous.

A number, d, of these can be used in the same form as (7) to deform an image but this scheme is not ideal [24]. However, as we are not using these coefficients to perform the whole deformation these problems are not applicable.

3. DEFORMATIONS INCORPORATING RIGID STRUCTURES

Our original problem is one where we wish to constrain parts of the image to be transformed subject to a predetermined rigid body transformation, while using landmarks outside the rigid bodies to define a deformation. As before let us have n landmark sites in $\mathbb{R}^d$ given by $\mathbf{t}_i = (t_i[1], \ldots, t_i[d])^T$ which we wish to transform to new sites $\mathbf{u}_i = (u_i[1], \ldots, u_i[d])^T$ under the deformation. If we just have landmarks then we can form an interpolating deformation given by (5)–(10). We can rewrite the top equation of (9) as

$$\Sigma B + DA = U. \tag{15}$$

We know Σ, D, and U, and the matrix A represents the linear part of the transformation. Hence if we can control A we can control the linear part of the deformation and hence constrain regions of $\mathbb{R}^d$ to have a prespecified linear transformation. If we combine this with a nonlinear deformation which is zero within these regions and tends toward zero as we move toward these regions then we can constrain rigid structures in our deformation.

First let us have n_o objects which we shall call O_i, $i = 1, \ldots, n_o$. Each O_i is a set of points in $\mathbb{R}^d$ which form a single rigid region. The objects may contain holes or even consist of two distinct regions which form part of the same rigid structure, but cannot be overlapping. We can then define an overall "object" set by $O_0 = O_1 \cup O_2 \cup \cdots \cup O_{n_o}$. Each of the individual objects has an associated linear transformation which constrains its motion. We shall denote these by the matrices L_i, $i = 1, \ldots, n_o$. Each L_i is a $d \times M$ matrix of coefficients which when combined with the M basis functions $g_j(\mathbf{t})$, $j = 1, \ldots, M$ form a linear transformation. Further let $\mathscr{D}_i(\mathbf{t})$, $i = 0, \ldots, n_o$ be a measure of the distance from the point $\mathbf{t}$ to the object O_i, which is zero for $\mathbf{t} \in O_i$, nonzero elsewhere, and continuous over $\mathbb{R}^d$.

It is possible to control the nonlinear deformation by careful selection of our basis function. We can define a basis function which tends to zero as we move toward any of the objects by weighting a valid basis function with the distance to the closest rigid body. For two points $\mathbf{t}$ and $\mathbf{t}_i$ this gives us

$$\sigma'(\mathbf{t}, \mathbf{t}_i) = \mathscr{D}_0(\mathbf{t})\mathscr{D}_0(\mathbf{t}_i)\sigma(\mathbf{t}, \mathbf{t}_i). \tag{16}$$

This will tend to zero as the point $\mathbf{t}$ tends to any image object. Further if we form the matrix Σ' where $\Sigma'_{ij} = \sigma'(\mathbf{t}_i, \mathbf{t}_j)$ using (16) then we can decompose it in the following manner:

$$\Sigma' = K\Sigma K,$$

where

$$K_{ij} = \begin{cases} \mathscr{D}_0(\mathbf{t}_i) \text{ if } i = j, \\ 0 \text{ otherwise} \end{cases} \quad \text{and } \Sigma_{ij} = \sigma(\mathbf{t}_i, \mathbf{t}_j)$$

as K is diagonal and $\mathscr{D}_0(\mathbf{t}_i) \neq 0$, as the landmarks are not on the objects, then K^{-1} exists. Hence, in order to ensure that Σ' is invertible we have to choose a $\sigma(\mathbf{t}, \mathbf{t}_i)$ which ensures that Σ is nonsingular and invertible. There are many functions which have this property [19, 21, 22].

In order to define our linear term we have used a weighted sum of each object's linear transformation. We shall use weights similar to (13) but with $s_i(\mathbf{t})$ replaced by $\mathscr{D}_i(\mathbf{t})$ giving

$$w_i(\mathbf{t}) = \frac{q_i(\mathbf{t})}{\sum_{j=1}^{n_o} q_j(\mathbf{t})},$$

where

$$q_i(\mathbf{t}) = \frac{1}{\mathscr{D}_i(\mathbf{t})^\mu}.$$

So we have

$$w_i(\mathbf{t}) = \begin{cases} 1 \text{ if } \mathbf{t} \in O_i \\ 0 \text{ if } \mathbf{t} \in O_j, \quad j = 1, \ldots, n_o, \quad j \neq i \end{cases} \tag{17}$$

and

$$\sum_{i=1}^{n_o} w_i(\mathbf{t}) = 1 \text{ for all } \mathbf{t}. \tag{18}$$

For any point $\mathbf{t}$ we define our linear transformation as

$$\mathscr{L}(\mathbf{t}) = \sum_{i=1}^{n_o} w_i(\mathbf{t}) L_i, \tag{19}$$

where (17) ensures the required linear transformation at the objects and (18) ensures the existence of the identity mapping; in this paper we shall take $\mu = 1.5$.

Using (19) to define our linear transformation we can rewrite the coefficient equation (15) as

$$B = \Sigma'^{-1}(U - T), \tag{20}$$

where

$$T = \begin{pmatrix} \mathbf{g}(\mathbf{t}_1)^T \mathscr{L}(\mathbf{t}_1)^T \\ \mathbf{g}(\mathbf{t}_2)^T \mathscr{L}(\mathbf{t}_2)^T \\ \vdots \\ \mathbf{g}(\mathbf{t}_n)^T \mathscr{L}(\mathbf{t}_n)^T \end{pmatrix} \tag{21}$$

and

$$\mathbf{g}(\mathbf{t}_i) = (g_1(\mathbf{t}_i), \ldots, g_M(\mathbf{t}_i))^T. \tag{22}$$

We can now write the interpolation solution for $\mathbb{R}^d \to \mathbb{R}^d$ in the following manner,

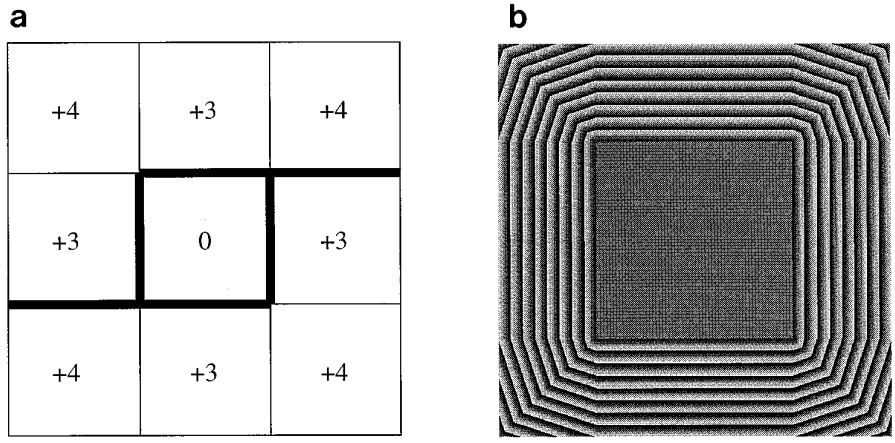

FIG. 1. A 3–4 distance transform: (a) the 3–4 DT mask; (b) the 3–4 DT of a square displayed with a cyclical grayscale colormap.

$$\mathbf{t} \to \mathbf{f}(\mathbf{t}) = \mathscr{L}(\mathbf{t})\mathbf{g}(\mathbf{t}) + \sum_{j=1}^{n} B_j^T \sigma'(\mathbf{t}, \mathbf{t}_j), \tag{23}$$

where B_j is the jth row of B given by (20), $\sigma'(\mathbf{t}, \mathbf{t}_i)$ is given by (16) and $\mathscr{L}(\mathbf{t})$ by (19).

4. APPLICATION TO IMAGES: DISTANCE TRANSFORMS

In order to apply this technique to discrete images we must evaluate the distance from any point to a segmented image structure which consists of a number of pixels or voxels. Distance transforms (DT) are algorithms developed to allow the distance, or an approximation of the distance, from any pixel or voxel to a predefined image feature to be easily obtained. They involve passing a mask over the image a number of times, generating an image in which each pixel contains a value that corresponds to the distance to the nearest feature pixel (Borgefors [25] includes a detailed review). A commonly used two-dimensional DT is the 3–4 DT [25, 26], and its mask is shown schematically in Fig. 1a. The 3–4 DT is found by first segmenting the image into object and background and then passing, first the upper half of the mask (above the solid line) in Fig. 1a including 0 forward over the image. The minimum of the current pixel value and the pixels which the mask covers plus their corresponding distance measure (either 3 or 4) is then assigned to the current pixel. Following this the lower portion of the mask, again including 0, is passed backward over the image and again the minimum value is assigned to the current pixel. The result of using this to form a distance transform of a square is shown in Fig. 1b with the distances plotted using a cyclical grayscale colormap. It is clear that the 3–4 DT produces artifacts at the corners of the square. This is caused by the pixellation of the square and the approximate distance measurement of the 3–4 DT.

A Euclidean distance transform (EDT) is a much more exact distance transform and it will assign the actual Euclidean distance to nearly all of the pixels or voxels in the image. One of the first two-dimensional EDTs was presented by Danielsson [27] and is based on a mask which is passed over the image and assigns a two-dimensional vector to each pixel. This makes it both slow and expensive in memory. It is because of this that we have chosen to use the fast Euclidean distance transform proposed by Huang and Mitchell [28]. This method is based on a decomposition of the Euclidean distance transformation structuring element into 3×3 windows; the mask used is shown in Fig. 2a. The mask changes for each iteration, i, and also incorporates the pixel dimensions $m \times n$ so that nonsquare pixels can be taken into consideration. This propagates from the edges of objects within the image; the original method [28] calculates the distance from a pixel within an object to the edge of the object. It is however simple to change the algorithm so that it calculates the distance from a pixel in the image to an object. We first segment the image into object and background with our object being assigned the value zero and the background a high value. The algorithm has an initialization step where the mask, with $i = 1$, is passed over the whole image and subtracted from the neighborhood of each pixel; the minimum value is then assigned to the central pixel. As this is a propagation technique only pixels whose neighbors changed in the previous iteration can change in the current iteration. Hence after the initial pass over the whole image only a small subset of the image pixels needs to be accessed in order to complete the next iteration. This increases the speed of the algorithm significantly. We continue the algorithm until enough iterations have been carried out so that the whole image plane has a distance value. The result of the trans-

a

$-2(m^2+n^2)i$ $+m^2+n^2$	$-2n^2i+n^2$	$-2(m^2+n^2)i$ $+m^2+n^2$
$-2m^2i+m^2$	0	$-2m^2i+m^2$
$-2(m^2+n^2)i$ $+m^2+n^2$	$-2n^2i+n^2$	$-2(m^2+n^2)i$ $+m^2+n^2$

b

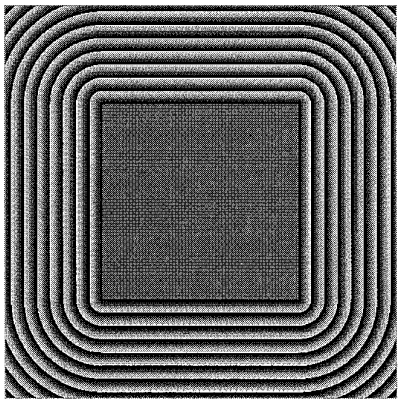

FIG. 2. An Euclidean distance transform based on a morphological operator: (a) the EDT mask, where m and n are the pixel dimensions and i is the iteration number; (b) an EDT of a square using $m = n = 1$ and displayed with a cyclical grayscale colormap.

form is an image where each pixel contains the square of the distance from it to the closest segmented structure and so this also requires less storage than the method of [27]. Figure 2b shows the result of evaluating the Euclidean distance transform outlined above on the same square as used in Fig. 1b, once again it is displayed with a cyclical grayscale colormap. It is clear that any artifacts due to the corners of the square are negligible.

5. RESULTS

In order to evaluate our deformations we must first choose a valid basis function. Ruprecht *et al.* [24] have experimented with a wide range of basis functions and have concluded that multiquadrics performed in a more satisfactory manner than other functions. We shall now show some illustrative examples using a Hardy multiquadric [29], which we have modified, as our basis function; this is given by

$$\sigma'(\mathbf{t}, \mathbf{t}_i) = \mathscr{D}_0(\mathbf{t})\mathscr{D}_0(\mathbf{t}_i)(|\mathbf{t} - \mathbf{t}_i|^2 + R_i^2)^{\alpha/2} \qquad (24)$$

and by using (19)–(23) to form our deformation. The choices of α and R_i are subjective, we have used $\alpha = 1$, as proposed by Hardy [29], and taken R_i to be the distance from landmark $\mathbf{t}_i$ to the closest rigid body. The R_i's act as locality parameters, when R_i is small the deformation will be more elastic than when R_i is large.

Figure 3 shows the results of using both standard landmark based deformation and a deformation incorporating a rigid structure. The original image, with the square in gray and 16 landmarks marked by black crosses, is plotted in Fig. 3a. We shall assume that we know that the square is a rigid structure and we shall attempt to rotate it through 45°. Figure 3b shows the result of using 8 of the 16 landmarks, one at each corner of the image and one at each corner of the square. The four image corners have been fixed and the four corners of the square have been rotated through 45° with respect to the center of the square. It is clear that if the square is known to be a rigid structure then we have a very unsatisfactory transformation. The image in Fig. 3c shows the result of using all 16 landmarks shown in Fig. 3a, once again the image corners are fixed and the remaining landmarks rotated through 45° with respect to the center of the square. The addition of extra landmarks has improved the transformation of the square but it is still obviously deformed. We could carry on adding landmarks until the square takes a more rigid shape or, taking landmarks to their extreme, use a landmark at every pixel within the square. This is however not a satisfactory solution as the addition of these extra landmarks soon makes the computational cost of the deformation prohibitive. Figure 3d shows the result of using (19)–(24) with one rigid body, the square, and 4 landmarks, the four corners of the image. We have set L_1 to be the coefficients required for a 45° rotation. It is clear that we have achieved the desired rotation of the square without any deformation of the object. This is a vast improvement over normal landmark-based techniques as well as being quick to compute (quicker than computing Fig. 3c).

The theory is valid for any number of rigid bodies and Fig. 4 shows two deformations of a simulated section of spine with five rigid bodies and four landmarks. The original image is Fig. 4a where the rigid bodies are the gray squares and we have a landmark at each of the four corners which we fix in position. Figure 4b shows a bending of the overall image; this is the sort of deformation one would expect in the spine where the squares could be thought of as the vertebrae. Here we have a smooth and reasonable deformation of the image surrounding the objects. In Fig.

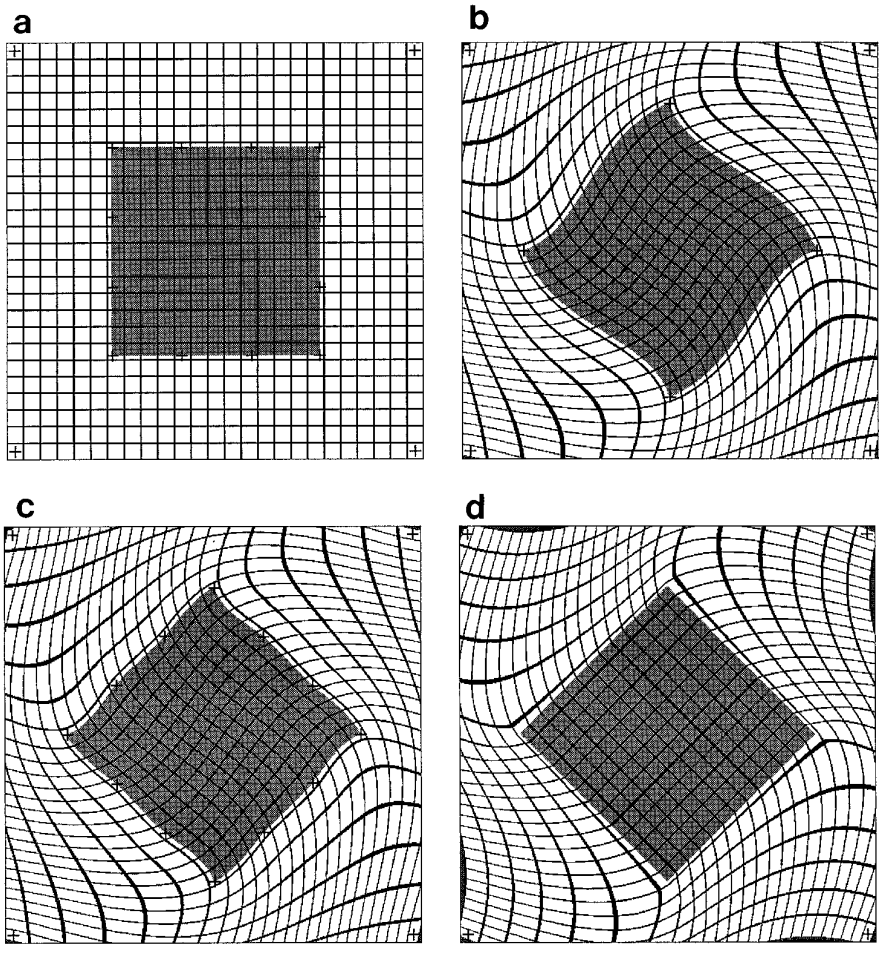

FIG. 3. The rotation through 45° of a ''rigid'' square within an image while keeping the image corners fixed: (a) the original square; (b) a transformation using 8 landmarks; (c) a transformation using 16 landmarks; (d) the transformation using 4 landmarks and one rigid object, the square.

4c we have moved the rigid bodies in a more random manner involving both translations and rotations. This image demonstrates the robustness of the algorithm to deformations which would not appear to be biologically reasonable. Deformations such as this may be difficult to model using a biomathematical model but could occur during a surgical procedure or due to a severe trauma.

Figure 5 shows the results of constructing a deformation incorporating rigid bodies for a sagittal MR image of the human spine. Figures 5a and 5b show a sagittal slice through the head and neck of a volunteer with their neck in different positions. We are now going to match the images together. Figures 5c and 5d show segmentations of Figs. 5a and 5b, respectively. These were achieved by drawing around the vertebrae and posterior of the skull by hand. We actually have nine rigid structures in this image; this is because the spinal processes, which appear to be separate from the spinal column, are in fact attached to vertebrae. We have also used 15 landmarks which are shown as white crosses in Figs. 5a and 5b. Figure 5e shows the result of matching the 15 landmarks and nine rigid bodies of Fig. 5a to those of Fig. 5b. The linear transformations were found by first matching the centers of gravity of the rigid bodies and then rotating them to the correct position. These were evaluated automatically from the segmented images by matching the principal axes of the shapes. This is not an ideal solution as it is susceptible to noise in the segmentations, although it does work in this example. In the future we will investigate different rigid body matching methods including chamfer matching. Figure 5f shows a thresholded boundary of Fig. 5e overlaid onto Fig. 5b. It is clear that we have achieved a high degree of accuracy for internal structures both at the rigid bodies and also in the surrounding deformable tissue, except at the skin surface which is not of clinical relevance.

6. CONCLUSIONS AND DISCUSSION

This paper provides a multidimensional interpolating technique for forming a deformation of $\mathbb{R}^d$ based on both

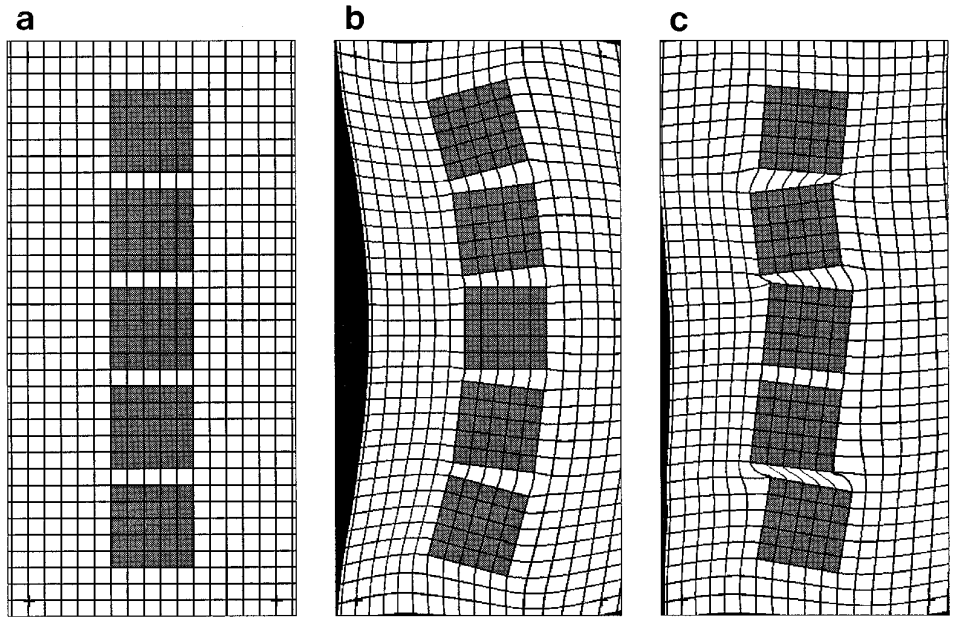

FIG. 4. A simulated section of spine comprising five separate rigid squares (vertebrae) (a) in their original positions, and after two deformations (b) and (c); in both cases the squares move rigidly as the spine deforms.

landmark and object constraints. The method transforms user-defined objects and landmarks exactly and provides a smooth interpolation elsewhere in the image. We have provided a number of illustrative examples to demonstrate the usefulness of this method.

We have chosen an interpolation approach with added constraints as a compromise between accuracy and speed of processing; all the figures in this paper took less than 6 min on a SUN SPARC 20/61 to compute. Model-based approaches can, if they are based on accurate image information, prove more accurate, but they are very computationally expensive. For interventional work we require a solution quickly (how quickly will depend on the interventional procedure) but not necessarily in real time as routinely there are periods of inactivity during a procedure.

This paper only contains examples on two-dimensional images but the theory is valid in three dimensions as well. The use of this technique on three-dimensional images will require the exploration of a number of important points. Slice thicknesses in the images will vary and the choice of distance transform may have to be made after taking this into account. The number of landmarks which must be chosen in order to obtain an accurate transformation also needs to be found. This will be dependent on the problem being studied and also how much deformation the user is trying to account for. One limitation of this technique is the necessity for image segmentation and landmark selection. Ideally it would be optimal to have a technique which selects the landmarks and segments the images automatically. There has recently been some work by Rohr *et al.* [31] where they automatically select landmarks and formulate an approximating thin-plate spline. A further addition to the algorithm would be the automatic matching of the rigid structures. We already have distance transforms of our images so a chamfer match should be possible. Also, work has already been carried out on using gray level correlation techniques to match a single vertebra from CT to an MR image (see [32]). Future communications will address these points for applications using three-dimensional medical images.

Unlike rigid body registration where the result is predictable at all points in the image, incorporating deformations could lead to misleading or inaccurate results, especially far from landmarks or identified rigid bodies. The choice of basis function affects the interpolation solution; however, in image deformation we do not know the ''correct'' interpolation scheme. In one deformation kriging may prove to be the best method; in another a thin-plate spline may be best or a radial basis function solution may prove to be the best. There is no way of predicting which basis function will fit the data best away from the landmarks as we are only given information at certain points in the image. Validation of this approach is therefore an important issue especially as it is hoped that these methods will find applications in surgical therapeutic interventions in order to improve the accuracy of image guidance. Validation will proceed by assessing the accuracy of transformation of structure boundaries and other features which have not been identified *a priori* as constraints. In certain circumstances it may also be possible to track structures

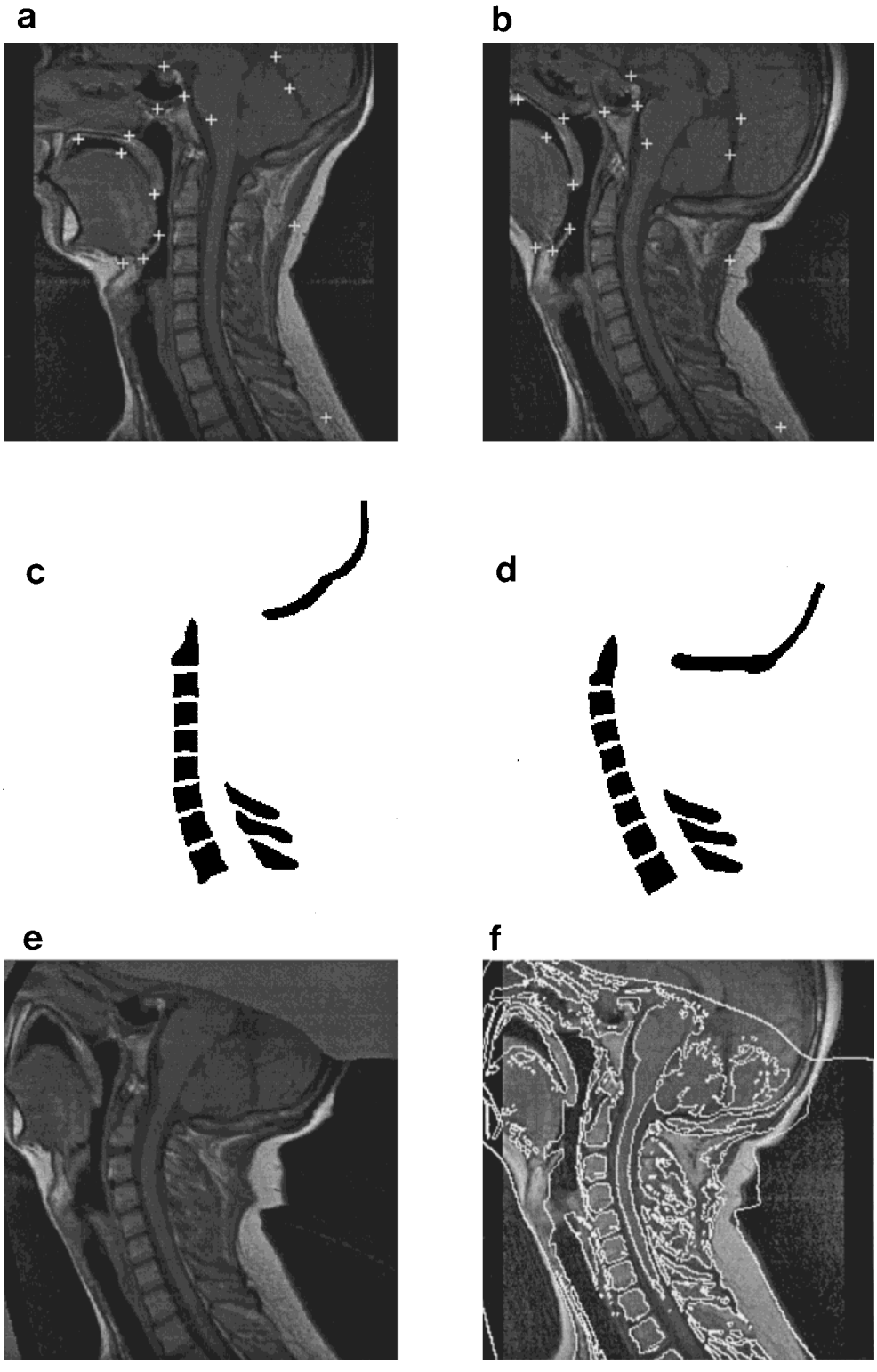

FIG. 5. An image match incorporating rigid structures: (a) the original image with landmarks; (b) the destination image with corresponding landmarks; (c) the segmentation of (a); (d) the segmentation of (b); (e) the result of deforming (a) using the landmarks of (a) and (b) and matching the rigid bodies in (c) and (d); (f) a threshold overlay of (e) onto (b).

such as surgical clips or other markers inserted during previous interventions. Detailed descriptions of our approaches to validation will be described in future submissions.

The use of derivative information can help to improve the accuracy of the transformation further (see [9, 30]). Our method can be extended to allow the use of derivative constraints at positions away from the rigid objects. Directional derivatives of the EDTs can be found numerically; μ in (14) can be chosen so that the weights are differentiable to the required order and the basis function $\sigma(\mathbf{t}, \mathbf{t}_i)$ and the order r of the underlying drift can be chosen using the method laid down for kriging with derivatives [13].

ACKNOWLEDGMENTS

We are grateful for the financial support of Philips Medical Systems (EasyVision/EasyGuide Advanced Development) (JAL) and the UK EPSRC (Grant GR/J90183) (DLGH, DJH). We also thank Paul Summers for this help with the MR data acquisition and the members of the Image Processing Group at Guy's Hospital and Prof. Kanti Mardia, Leeds University, for useful discussions. The support and encouragement of Prof. Andreas Adam and Dr. John Reidy is also greatly appreciated.

REFERENCES

1. P. A. van den Elsen, E. J. D. Pol, and M. A. Viergever, Medical image matching—A review with classification, *IEEE Eng. Med. Biol.* March 1993, 26–39.
2. C. R. Maurer, Jr. and J. M. Fitzpatrick, A review of medical image registration, in *Interactive Image-Guided Neurosurgery* (R. J. Macuinas, Ed.), pp. 17–44, Am. Assoc. Neurological Surgeons, Park Ridge, IL, 1993.
3. N. Ayache, Medical computer vision, virtual reality and robotics, *Image Vis. Comput.* **13**(4), 1995, 295–313.
4. S. Lavallee, Registration for computer-integrated surgery, in *Computer-Integrated Surgery* (R. H. Taylor, S. Lavallee, G. C. Burdea, Eds.), pp. 77–97, MIT Press, Cambridge, MA, 1995.
5. D. L. G. Hill, D. J. Hawkes, J. E. Crossman, M. J. Gleeson, *et al.*, Registration of MR and CT images for skull base surgery using point-like anatomical features, *Br. J. Radiol.* **64,** 1991, 1030–1035.
6. R. P. Woods, J. C. Mazziotta, and S. R. Cherry, MRI–PET registration with automated algorithm, *J. Comput. Assist. Tomogr.* **17**(4), 1993, 536–546.
7. P. Viola and W. M. Wells, Alignment by maximization of mutual information, in *Proceedings of the 5th International Conference on Computer Vision, 1995,* pp. 16–23.
8. C. Studholme, D. L. G. Hill, and D. J. Hawkes, Multi resolution voxel similarity measures for MR–PET registration, in *Information Processing in Medical Imaging* (Y. Bizais, C. Barillot, and R. di Paola, Eds.), pp. 287–298, Kluwer, Dordrecht, 1995.
9. K. V. Mardia and J. A. Little, Image warping using derivative information, in *Mathematical Methods in Medical Imaging. III. SPIE, Vol. 2099, San Diego, CA, 1994,* (F. L. Bookstein, J. S. Duncan, N. Lange, and D. C. Wilson, Eds.), pp. 16–31.
10. P. J. Edwards, D. L. G. Hill, J. A. Little, V. A. S. Sahni, *et al.,* Medical image registration incorporating deformations, in *British Machine Vision Conference, 1995* (D. Pycock, Ed.), pp. 691–699.
11. K. Waters, A physical model of facial tissue and muscle articulation derived from computer tomography data, in *Visualization in Biomedical Computing, Proc. SPIE, Vol. 1808* (R. A. Robb, Ed.), pp. 574–583, 1992.
12. C. A. Christenson, R. D. Rabbitt, M. I. Miller, S. C. Joshi, *et al.*, Topological properties of smooth anatomic maps, in *Information Processing in Medical Imaging* (Y. Bizais, C. Barillot, and R. Di Paola, Eds.), pp. 101–112, Kluwer, Dordrecht, 1995.
13. K. V. Mardia, J. T. Kent, C. R. Goodall, and J. A. Little, Kriging and splines with derivative information, *Biometrika* **83**(1), 1996, 207–221.
14. F. L. Bookstein, Principal warps: Thin-plate splines and the decomposition of deformations, *IEEE Trans. Patt. Anal. Mach. Intell.* **11,** 1989, 567–585.
15. F. L. Bookstein, Thin-plate splines and the atlas problem for biomedical images, in *Information Processing in Medical Imaging* (A. C. F. Colchester and D. J. Hawkes, Eds.), pp. 326–342, Kluwer, Dordrecht, 1991.
16. N. Arad, N. Dyn, D. Reisfeld, and Y. Yeshurun, Imaging warping by radial basis functions: Application to facial expression, *CVGIP: Graphic. Models Image Process.* **56**(2), 1994, 161–172.
17. N. Arad and D. Reisfeld, Image warping using few anchor points and radial functions, *Comput. Graph. Forum* **14**(1), 1995, 35–46.
18. D. Shepard, A two-dimensional interpolation function for irregularly spaced data, in *Proceedings, 23rd National Conference of the ACM,* pp. 517–524, ACM Press, New York, 1968.
19. D. E. Myers, Kriging, cokriging, radial basis functions and the role of positive definiteness, *Comput. Math. Applic.* **24**(12), 1992, 139–148.
20. N. A. C. Cressie, *Statistics for Spatial Data,* second ed., Wiley, New York, 1993.
21. C. A. Micchelli, Interpolation of scattered data: Distance matrices and conditionally positive definite functions, *Constructive Approximation* **2,** 1986, 11–22.
22. G. Wahba, *Spline Models for Observational Data,* Society for Industrial and Applied Mathematics, Philadelphia, 1990.
23. F. L. Bookstein, *Morphometric Tools for Landmark Data,* Cambridge Univ. Press, Cambridge, UK, 1991.
24. D. Ruprecht, R. Nagel, and H. Müller, Spatial free-form deformation with scattered data interpolation methods, *Comput. Graph.* **19**(1), 1995, 63–71.
25. G. Borgefors, Distance transformations in digital images, *Comput. Vis. Graph. Image Process.* **34,** 1986, 344–371.
26. D. L. G. Hill and D. J. Hawkes, Medical image registration using knowledge of adjacency of anatomical structures, *Image Vis. Computing* **12,** 1994, 173–178.
27. P. Danielsson, Euclidian distance mapping, *Comput. Graph. Image Process.* **14,** 1980, 227–248.
28. C. T. Huang and O. R. Mitchell, A Euclidean distance transform using grayscale morphology decomposition, *IEEE PAMI* **16**(4), 1994, 443–448.
29. R. L. Hardy, Multiquadric equations of topography and other irregular surfaces, *J. Geophys. Res.* **76**(8), 1971, 1905–1915.
30. F. L. Bookstein and W. D. K. Green, A feature space for edgels in images with landmarks, *J. Math. Imag. Vis.* **3,** 1993, 231–261.
31. K. Rohr, H. S. Stiehl, R. Sprengel, W. Beil, *et al.*, Point-based elastic registration of medical image data using approximating thin-plate splines, in *Visualization in Biomedical Computing* (K. H. Hohne and R. Kikinis, Eds.), pp. 297–306, Springer-Verlag, Berlin, 1996.
32. P. A. van den Elsen, E. J. D. Pol, T. S. Sumanaweera, P. F. Hemler, *et al.*, Grey value correlation techniques used for automatic matching of CT and MR brain and spine images, in *Proceedings of Visualization in Biomedical Computing, 1994, SPIE Proceedings, Vol. 2359,* (R. A. Robb, Ed.), pp. 227–237.